A Deep Learning Technique for Detecting High Impedance Faults in Medium Voltage Distribution Networks

S. Lavanya
Department of Electrical and Electronics Engineering
Sri Chandrasekharendra Saraswathi Viswa Mahavidyalaya
Kanchipuram, Tamilnadu, India
lavanya@kanchiuniv.ac.in

S. Prabakaran
Department of Electrical and Electronics Engineering
Sri Chandrasekharendra Saraswathi Viswa Mahavidyalaya
Kanchipuram, Tamilnadu, India
prabakaran@kanchiuniv.ac.in

N. Ashok Kumar
Department of Electrical and Electronics Engineering
Sri Chandrasekharendra Saraswathi Viswa Mahavidyalaya
Kanchipuram, Tamilnadu, India
ashokeee@kanchiuniv.ac.in

Received: 29 August 2022 | Revised: 8 September 2022 | Accepted: 9 September 2022

Abstract-Utility companies always struggle with the High Impedance Fault (HIF) in the electrical distribution systems. In this article, the current signal is seen in situations involving 10,400 different samples, with and without HIF, like linear, non-linear load, and capacitance switching. A better method that processes signals very fast and with low sample rates, requiring less memory and computational labor, is demonstrated by Mathematical Morphology (MM). For HIF identification, Deep Convolution Neural Networks (DCNNs) are being developed. This paper presents a novel method for signal processing with low sample rates, high signal processing speed, and low computational and memory requirements. The suggested six-layer DCNN is compared with other models, such as the four-layer and eight-layer DCNN models and the results are discussed.

Keywords-high impedance fault; mathematical morpologhy; deep convolution neural networks

I. INTRODUCTION

For a power system to operate securely and dependably, an adequate protective mechanism that can recognize, classify, and locate the system's defects is essential. Even though standard protection relays are able to quickly recognize low-impedance network faults [1-3], but they can't notice HIFs' small fault current, something that represents a significant safety threat**.** In addition, the power network experiences cascading failures as a result of the HIFs spreading into a functioning area of the grid system. Therefore, HIF detection is very important in a distribution system. Feature extraction and classifier development are the first two steps in the detection of HIF.

Numerous Signal Processing Techniques (SPTs) have been presented to extract features for the purpose of training and testing classifiers during the pattern recognition stage using time-frequency transforms to obtain the proper patterns. This technique separates the different disturbances. The Fast Fourier Transform (FFT) includes information on signal loss and the time loss while analyzing the data for feature extraction [4, 5]. The Short Time Fourier Transform (STFT) has been often used for fault analysis. It is, however, inadequate for evaluating non-stationary transient signals that have both temporal and frequency components due to its constant window length. Time-frequency analysis performs well across all detection criteria and is particularly sensitive to non-stationary signals. However, the length of the computations raises questions about the technology's suitability for protection applications. The signal can be processed using the Wavelet Transform (WT) approach by examining its low- and high-frequency components. Using the wavelet decomposition coefficient of a voltage waveform, a WT-based approach may identify HIFs. Wavelet packet transform is applied to features extracted from voltage and current signal data in order to identify and distinguish HIFs. The level 5 and level 7 approximation coefficients as well as the standard deviation of detail of the db4 mother wavelet are employed for such detection process. WT offers greater signal processing resolution. However, the implementation of this approach in protective applications is limited by its high computational complexity, high data rate, and storage space requirements [6]. Recently, Mathematical Morphology (MM) was used in HIF detection, although the technique needs to be improved.

The majority of detection techniques observe the input signal for processing while selecting a high sample rate. High sampling rates increase the amount of the needed computational space. The current study shows an improved technique that processes signals extremely quickly and with

Corresponding author: S. Lavanya

low sampling rates, which requires less memory and computational work. To gather the HIF and non-HIF current signal data, a precise MATLAB/SIMULINK model of a genuine power distribution network was used. MM is a time-domain, nonlinear signal transformation technique. Processing time is reduced because of the usage of simpler calculations [7, 8]. Additionally, MM filters are appropriate for real-time power system activities like transmission line protection. The most important task in the signal processing technique is the extraction of critical features, which is made possible by the interaction between the signal and the Structured Element (SE). SE shape plays a key role in signal processing. The MM filter is used in this study to pre-process the current signal. While preserving fault current characteristics, this filter lowers the signal's noise level.

Deep Learning (DL) is very good at automatically extracting features from speech and image analysis. DL can capture both temporal and spatial data from the input without the need for signal manipulation [9-11]. By removing manually created feature extraction, the use of DL in fault and non-fault detection not only increases accuracy, but also streamlines the process. Convolution Neural Networks (CNNs) were used to solve the high impedance fault problem, and performance against noise, training time, parameter count, and overall performance have all been discussed. For the purpose of detection and classification, a Deep Convolution Neural Network (DCNN) receives a 2D image that has been converted from the fault and non-fault signal. The 1D signal data and the 2D signal image are completely different things [12-14].

Previous literature has not taken into account multiple power quality disturbances. The proposed method is using DCNN for the problem of multiple fault and non-fault detection and signal classification. The MM filter is used in this study to pre-process fault and non-fault current signals while maintaining fault current characteristics [15-18]. This filter reduces the signal noise level. Then, using a CNN, the output signal of the mathematical morphology with and without faults is detected. The following is a list of the current study's contributions.

- By analyzing the fault and non-fault MM output signal, the DCNN layer minimizes the manual extraction of features and permits automatic feature extraction.
- Due to the high computational complexity of the CNN, a Batch Normalization (BN) layer is implemented to speed up the training procedure and minimize the number of parameters.

II. THE MATHEMATICAL MORPHOPOLOGY

The structure of signals is altered via a non-linear signal processing method termed MM. This method was created in its natural shape in 1975. Integral geometry and set theory are the foundations of MM. MM operates entirely in the time domain and does not compute the frequency content of a signal, as opposed to Fourier or wavelet transforms, which separate the signals' frequency information. Recently, MM has been applied to power distribution systems, particularly for fault identification [19, 20]. As a result, an effort has been made to leverage MM in pre-processing the signals in order to lessen the workload on the computer, the amount of memory needed, and the overall detection latency. The SE is the foundation of the MM processing applications. For the execution of any MM-based operation, the choice of SE is a crucial step. The type and frequency content of the fault signal affect the choice of SE. Erosion and dilation are two essential MM changes [21, 22]. These two transformations can be creatively coupled to create other transformations that can be applied in the right situations. It has been stated that various MM-based tools are used for power system applications [23]. These instruments are produced using a variety of replications and mixes of dilation and erosion employing various structuring components [24].

A. The Choice of a Structuring Element

The SE is a necessary component of MM-based signal processing. It is an operator used in signal processing that separates a signal into sub-signals of various important properties. Depending on the types of applications, it could have different geometrical structures [25]. The one-dimensional signals obtained from power systems are examined using linear SEs. Signal transformations depend significantly on the SEs' length and height (magnitude).

B. Structuring Element Length

The window size for any MM function is determined by the length of a SE, which also determines the delayed in output. With respect to the MM operation, the output delay is equal to (m-1) ΔT, where T is the sampling interval, and m is the length of the SE. It should be observed that the output delay constantly grows as the SE lengthens. Therefore, linear SE with a length of 3 has been regarded as the best for fault detection applications in order to decrease time in MM transformations.

C. Structuring Element Height

In power systems, various current and voltage densities are employed. Therefore, the samples of current or voltage signals must be standardized using the peak magnitude of their rating value before MM modifications in order to have a more general option of the SE. In normal conditions, the normalization limits the signal magnitude to roughly 1 despite the various system voltage and current levels. As a result, a SE will always be at its best for any voltage or current levels. The magnitude (or height) of each SE element can be any small arbitrary value once the waveform has been adjusted [26].

III. THE FILTERS OF MATHEMATICAL MORPHORLOGY

Assume that X(n) is a signal that needs to be translated and specified in the domain $Dx = \{a_0, a_1...a_n\}$ and Y(m) is a SE defined in the domain $Dy = \{b_0, b_1....b_m\}$. The Dilation (+) of the signal X(n) by Y(m) is given by:

$$\text{Dilation}(n) = (X(n)+Y(m))=\text{Max}\{X(n-m)+Y(m)\} \quad (1)$$

where $0 \leq (n-m) \leq n$, $m \geq 0$, $n > m$, and n, m are integers.

The Erosion (-) of signal X(n) by Y(m) is given in (2):

$$\text{Erosion}(n) = (X(n)–Y(m))=\text{Min}\{X(n+m)–y(m)\} \quad (2)$$

where $0 \leq (n+m) \leq n$, $m \geq 0$.

As indicated above, the opening (α) and closing (+) functions are defined based on (1), (2) in (3) and (4) respectively.

$$\text{Opening } (n) = (X(n)@Y(m))=[(X(n)+Y(n))–Y(m)] \quad (3)$$

$$\text{Closing } (n) = (X(n)*Y(m))=[(X(n)-Y(m))+Y(m)] \quad (4)$$

Different Mathematical Morphological Filters (MMFs) are developed from these MM functions and employed in real-time signal processing applications. Closing – Opening(0) and Opening – Closing(α) are defined by:

$$Co(n) = (X(n) * Y(m)) @ Y(m) \quad (5)$$

$$Oc(n) = (X(n) @ Y(m)) * Y(m) \quad (6)$$

The Mean Closure – Opening Filter (MCOF) is designed as the arithmetic mean of close and open:

$$MCOF(n) = [Opening(n) + Closing(n)]/2 \quad (7)$$

The Mean Closing – Opening and Opening – Closing Filter (MCOOCF) is the mathematical mean of Co and Oc:

$$MCOOCF(n) = [Co(n) + Oc(n)]/2 \quad (8)$$

IV. SYSTEM DESCRIPTION

Authors in [5, 6] analyzed HIF with non-HIF scenarios using the 33KV feeder model shown in Figure 1. This model has a distribution transformer connecting its 11KV bus to its 33KV bus. The feeders in a subsystem model have seven numbers. The sixth feeder serves as a candidate feeder. Both HIF and non-impedance fault conditions were applied to this model to analyze the capacitance switching and non-linear loads for non-high impedance fault circumstances.

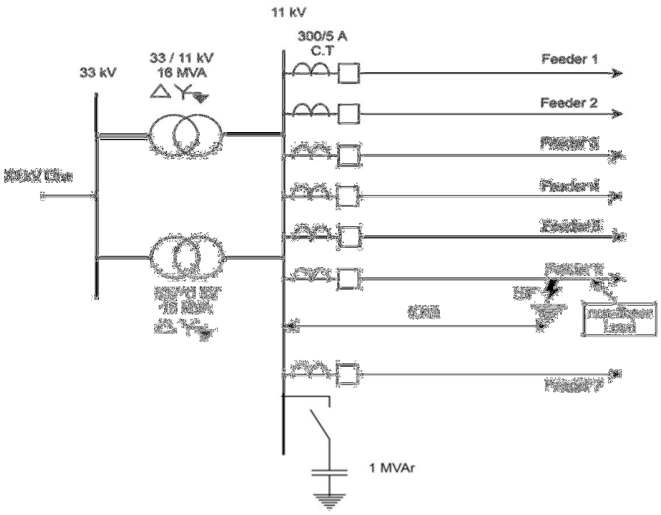

Fig. 1. System fescription.

A. Fault and Non-fault Signal Data

In this work, both kinds of distribution signals—fault and non-fault signal data—are taken into account. The non-fault signal data represent normal switching, load switching, and capacitance switching, while the fault signal data represents the HIF [27]. The data set, which is obtained from various simulation cases taken into account and is shown in Table I, is used in the proposed fault and non-fault signal detection method [28].

TABLE I. VARIOUS SIMULATION HIF AND NON-HIF CASES

Event	Simulation conditions	Total cases
HIF	Resistance of the HIF model varied from 100 to12k. The HIF model's DC voltage varied from 1kV to 11kV. Angle of origin of the fault at 0°, 30°, 45°, 60°, 90°. Phase angles of the source voltage are 0°, 30°, 45°, and 60°.	1500 (60×5×5)
Switching loads	Load level changes at 10 cases. Angle changes in a cycle of 0°, 30°, 45°, and 60°. Phase angles of the source voltage are 0°, 30°, 45°, and 60°.	250 (10×5×5)
Switching of nonlinear loads	NLL load level changes at 24 cases. Angle changes in a cycle of 0°, 30°, 45°, and 60°. Phase angles of the source voltage are 0°, 30°, 45°, and 60°.	600 (24×5×5)
Switching of capacitance	Switching a 1MVAr on and off depending on the load. Angle changes in a cycle of 0°, 30°, 45°, and 60°. Phase angles of the source voltage are 0°, 30°, 45°, and 60°.	250 (5×2×5×5)

A total of 1500 HIF cases and 1100 non-HIF cases, such as linear load switching, Non-Linear Load (NLL) switching, and capacitor switching, were considered (Table I). The generated signal has 2600 sampling points and a fundamental frequency of 50Hz (10 cycles, 0.2s). Data have been produced in each fault (1500) and non-fault (1100) case using different parameters. Thus, a total of 2600 sample points of fault and non-fault signal data examples have been produced. However, when the signal is actually acquired from the actual system through sensors, additional distortion is always imposed on the signal. Signal-to-Noise Ratios (SNRs) of 20dB to 40dB are added to the fault and non-fault signal data set in order to bring the total number of data samples up to 10,400. The specifications of the data set used in this analysis are listed in Table II.

TABLE II. THE DATA SET

	Counting samples	Quantity of noise
Training Set	2600*4 = 10,400	20 db - 40 db
Validation set	10,400*0.01 =104	20 db - 40 db
Test set	10,400*0.01 =104	20 db - 40 db

B. The Convolution Layer

The main layer in CNN is the Convolution Layer (CL), in which low-level features are transformed into high-level features. In order to create features, a kernel is used with the convolution operator on the input. The following is the CL's output:

$$y = f(Wr * xi + br)$$

where y is the result of CL. The weight and bias of the r^{th} layer are w^r and b^r respectively, and the activation function is f(x). It understands how a neuron becomes active and produces. The tanh function is not chosen in DL, but rather the rectified linear unit - activation functions.

$$f_{ReLU} = \max(0, y)$$

C. Pooling Layer

Usually, the CL is followed by a pooling layer. Its primary use is in down sampling. The pooling layer is used to decrease the dimension of the input and retrieve crucial information after the CL. It can lessen the effects of data volatility. Max pooling is used in this work because it performs better than average pooling for both fault and non-fault waveforms. The mathematical formula for max pooling is:

$$f(y) = \max_i (y_i)$$

D. BN Layer

The BN method is used for to speed up neural networks. It is used to normalize the input by altering and scaling the activations. Unlike the previous layers, it allows each network to learn independently. Additionally, compared to dropout, it efficiently reduces over fitting. The following formula can be used to normalize the input data batch x_i:

$$y_i = \gamma * \frac{x_i - \mu_x}{\sqrt{\varepsilon + \sigma_x^2}} + \beta$$

where σ_x^2 represents the batch variance and μ_x represents the batch mean. γ and β provide the learned scale and shift parameters respectively, guaranteeing that the input data have the same distribution.

E. Completely Joined Layer

The learning parameter D is included in this layer, which is also known as a "dense layer." The output of the dense layer is calculated using the formula below:

$$y = f(x * D^r + b^r)$$

F. SoftMax Layer

The probability distribution of each output class with "n" outputs is computed by the softmax layer. Thus, the softmax layer predicts the class to which the input data belong. The probability distribution is calculated using the following equation:

$$P_i = \frac{e^{x_i}}{\sum e^{x_j}}, \quad j = 0,1,2, \ldots\ldots\ldots n$$

where the input is x_i. The sum of all probabilities will equal to 1 if the output of p is between 0 and 1. In this work, fault and non-fault classification is done using the softmax layer [29].

V. THE PROPOSED METHOD-DCNN ALGORITHM

Figure 2 shows the proposed DCNN model's structure, which consists of two completely connected dense layers at the end of three convolution layers with pooling layers layered on top.

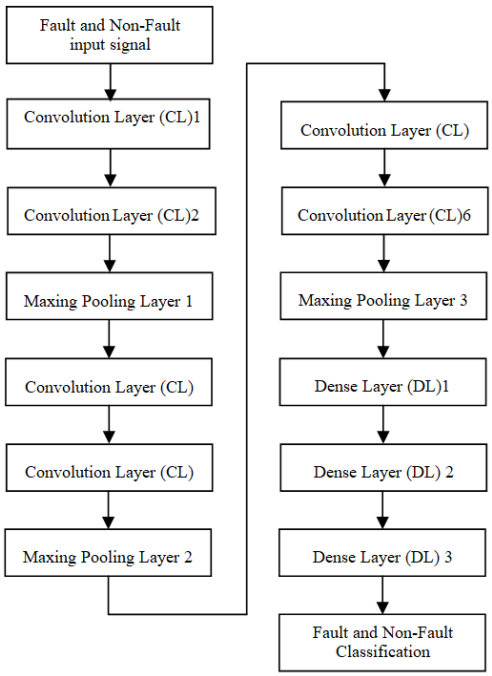

Fig. 2. The proposed DCNN architecture.

VI. SIMULATION RESULTS

A. Assessment Metrics

The proposed method was evaluated with the following criteria:

- The confusion chart is employed to evaluate a model's capability for classification.
- Accuracy is calculated as (true positive + true negative)/ total test instances.
- The product of the true positive and true negative determines precision.
- Recall equals the product of true positives and false negatives.
- The F1 score is determined as:

(Precision + Recall) 2 × Precision

B. Results and Discussion

As stated above, 10,400 samples have initially been created. One percent is utilized for validation, 1% for testing, and 98% of the total data set were used for training. In DL, the training process is often carried out using a small batch. In order to appropriately calculate the training time for various scenarios, the mini-batch size for all 3 DCNN cases is set at 64. A total of 100 epochs of validation loss were tracked. In order to avoid over fitting, the training method would be completed before the scheduled epochs, since the validation loss does not decrease continuously for 20 epochs. The final model is determined by whatever model performed best in the validation set. The suggested DCNN's entire architecture was coded in Python using a Tesla K80GPU in this study.

All models' accuracy and loss values during training are calculated using the DCNN with 4, 6, and 8 layers. Table III shows the 3 final models' variables, training period, number of epochs that have passed, accuracy level, and validation losses.

TABLE III. DCNN TRAINING MODEL PERFORMANCE

Model type	Epoch's duration (s)	Optimum validation losses	Maximum validation precision	Epochs
DCNN with 4 layers	32	0.0038	0.98	49
DCNN with 6 layers	46	0.0022	0.999	32
DCNN with 8 layers	72	0.003	0.996	36

Less training parameters and classification accuracy of 99.9% are produced by the 6-layer DCNN model. The confusion matrices for each of these DCNN models, HIF (600 samples) and non-HIF (440 samples), which were trained on a total of 1040 samples, are shown in Tables IV-VI. The DCNN with 6 layers correctly identified 600 HIF samples, with 0 samples being misclassified, yielding a 99.99% accuracy rate. A total of 592 HIF samples were accurately diagnosed by the 4-layer model, whereas 8 samples were incorrectly classified, giving it a classification accuracy of 98%. Also, 598 HIF instances were accurately diagnosed by the 8-layer DCNN model, whereas 2 samples were incorrectly classified, yielding a classification accuracy of 99.6%.

TABLE IV. DCNN6's CONFUSION MATRIX

Actual event	Predicted	
	HIFs	NHIFs
HIFs	600	0
NHIFs	1	439

TABLE V. DCNN8's CONFUSION MATRIX

Actual event	Predicted	
	HIFs	NHIFs
HIFs	598	2
NHIFs	2	438

TABLE VI. DCNN4's CONFUSION MATRIX

Actual event	Predicted	
	HIFs	NHIFs
HIFs	592	8
NHIFs	12	428

Table VII displays the precision, recall, and F1 score performance of the 6-layer DCNN model. While the 4-layer and 8 layer DCNN models generated 98.66% and 99.6% precision respectively, the suggested 6-layer model delivers 100% precision. Similar to this, the F1 score for a DCNN with 6 layers is 99.9%, compared to 98.33% and 99.66% of the 4- and 8-layer models respectively. As a result, the proposed 6-layer DCNN model outperformed the competition in terms of the evaluation parameters. Also, the 6-layer DCNN method outperforms the other models when compared to noisy environments. This approach reduces the detection delay to 23.66ms, making real-time applications possible.

TABLE VII. PARAMETERS OF EVALUATION OF THE THREE MODELS

Actual Event	DCNN 4		
	Precision	**Recall**	**F1 score**
HIFs	0.98666667	0.9801325	0.9833887
Actual Event	**DCNN 6**		
	Precision	**Recall**	**F1 score**
HIFs	1	0.99833611	0.99917
Actual Event	**DCNN 8**		
	Precision	**Recall**	**F1 score**
HIFs	0.99666667	0.99666667	0.99667

C. Comparing the Computation Lengths

To get greater performance, the DCNNs may be run on GPU. The GPU processor has more overall units than the CPU processor. As a result, DCNN computations run relatively quickly on a GPU. Due to its simultaneous GPU calculation, DCNN has a significantly shorter computation time. Table VIII compares the computation times on the GPU and CPU for the DCNN models using 2600 and 10400 samples.

TABLE VIII. PROCESSOR EFFECT ON TRAINING DURATION

Processor	Time interval (s)	
	2600 examples are included	10400 examples are included
Tesla K80 GPU	6	24
Intel i7 processor, CPU	18	72

VI. CONCLUSION

In order to classify HIFs and non-HIFs, this study suggests the use of a 6-layer DCNN model. The study demonstrates a new method that processes signals very quickly, with low sampling rates and reduced computational and memory load. The suggested DCNN with 6 layers is compared with other models, namely the 4- and 8-layer DCNN models. The findings show that the proposed 6-layer DCNN model has a greater accuracy while requiring less training than the other models. The 6-layer DCNN model outperforms the other models in noisy environments, it has fewer parameters, and is more convoluted. Future research will use the DCNN model to take into account more system faults.

REFERENCES

[1] A. Lazkano, J. Ruiz, L. A. Leturiondo, and E. Aramendi, "High impedance arcing fault detector for three-wire power distribution networks," in *10th Mediterranean Electrotechnical Conference. Information Technology and Electrotechnology for the Mediterranean Countries. Proceedings. MeleCon 2000 (Cat. No.00CH37099)*, Lemesos, Cyprus, Dec. 2000, vol. 3, pp. 899–902 vol.3, https://doi.org/10.1109/MELCON.2000.879677.

[2] N. Narasimhulu, D. V. Ashok Kumar, and M. V. Kumar, "Classification of high impedance fault using MWT and enhanced fuzzy logic controller in power system," in *Innovations in Power and Advanced Computing Technologies (i-PACT)*, Vellore, India, Apr. 2017, pp. 1–13, https://doi.org/10.1109/IPACT.2017.8244946.

[3] A.-R. Sedighi, M.-R. Haghifam, and O. P. Malik, "Soft computing applications in high impedance fault detection in distribution systems," *Electric Power Systems Research*, vol. 76, no. 1, pp. 136–144, Sep. 2005, https://doi.org/10.1016/j.epsr.2005.05.004.

[4] A. Aljohani, "Centralized Fault Detection and Classification for Motor Power Distribution Centers Utilizing MLP-NN and Stockwell Transform," in *IEEE PES Innovative Smart Grid Technologies Europe*

(ISGT-Europe), The Hague, Netherlands, Oct. 2020, pp. 222–226, https://doi.org/10.1109/ISGT-Europe47291.2020.9248886.

[5] K. Sekar and N. K. Mohanty, "Combined Mathematical Morphology and Data Mining Based High Impedance Fault Detection," *Energy Procedia*, vol. 117, pp. 417–423, Jun. 2017, https://doi.org/10.1016/j.egypro.2017.05.161.

[6] K. Sekar and N. K. Mohanty, "A fuzzy rule base approach for High Impedance Fault detection in distribution system using Morphology Gradient filter," *Journal of King Saud University - Engineering Sciences*, vol. 32, no. 3, pp. 177–185, Mar. 2020, https://doi.org/10.1016/j.jksues.2018.12.001.

[7] M. V. Reddy and R. Sodhi, "A rule-based S-Transform and AdaBoost based approach for power quality assessment," *Electric Power Systems Research*, vol. 134, pp. 66–79, May 2016, https://doi.org/10.1016/j.epsr.2016.01.003.

[8] A. H. A. Bakar, M. S. Ali, C. Tan, H. Mokhlis, H. Arof, and H. A. Illias, "High impedance fault location in 11kV underground distribution systems using wavelet transforms," *International Journal of Electrical Power & Energy Systems*, vol. 55, pp. 723–730, Feb. 2014, https://doi.org/10.1016/j.ijepes.2013.10.003.

[9] M. Mishra and P. K. Rout, "Detection and classification of micro-grid faults based on HHT and machine learning techniques," *IET Generation, Transmission & Distribution*, vol. 12, no. 2, pp. 388–397, 2018, https://doi.org/10.1049/iet-gtd.2017.0502.

[10] B. K. Chaitanya, A. Yadav, and M. Pazoki, "An Intelligent Detection of High-Impedance Faults for Distribution Lines Integrated With Distributed Generators," *IEEE Systems Journal*, vol. 14, no. 1, pp. 870–879, Mar. 2020, https://doi.org/10.1109/JSYST.2019.2911529.

[11] L. G. de Oliveira, M. de L. Filomeno, L. F. Colla, H. Vincent Poor, and M. V. Ribeiro, "Analysis of typical PLC pulses for sensing high-impedance faults based on time-domain reflectometry," *International Journal of Electrical Power & Energy Systems*, vol. 135, Feb. 2022, Art. no. 107168, https://doi.org/10.1016/j.ijepes.2021.107168.

[12] S. Gautam and S. M. Brahma, "Detection of High Impedance Fault in Power Distribution Systems Using Mathematical Morphology," *IEEE Transactions on Power Systems*, vol. 28, no. 2, pp. 1226–1234, Feb. 2013, https://doi.org/10.1109/TPWRS.2012.2215630.

[13] K. Rai, F. Hojatpanah, F. B. Ajaei, J. M. Guerrero, and K. Grolinger, "Deep learning for high-impedance fault detection and classification: transformer-CNN," *Neural Computing and Applications*, vol. 34, no. 16, pp. 14067–14084, Aug. 2022, https://doi.org/10.1007/s00521-022-07219-z.

[14] D. Pylarinos and I. Pellas, "Investigation of an Insulator Flashunder in an 150 kV OTL of the Power System of Crete," *Engineering, Technology & Applied Science Research*, vol. 9, no. 5, pp. 4851–4858, Oct. 2019, https://doi.org/10.48084/etasr.3198.

[15] S. R. Samantaray, "Decision tree-initialised fuzzy rule-based approach for power quality events classification," *IET Generation, Transmission & Distribution*, vol. 4, no. 4, pp. 538–551, Apr. 2010, https://doi.org/10.1049/iet-gtd.2009.0508.

[16] S. Kavaskar and N. K. Mohanty, "Detection of High Impedance Fault in Distribution Networks," *Ain Shams Engineering Journal*, vol. 10, no. 1, pp. 5–13, Mar. 2019, https://doi.org/10.1016/j.asej.2018.04.006.

[17] S. Lavanya, S. Prabakaran, and N. Ashok Kumar, "Behavioral Dynamics of High Impedance Fault Under Different Line Parameters," *International Journal of Electrical and Electronics Research*, vol. 10, no. 2, pp. 370–374, Jun. 2022, https://doi.org/10.37391/ijeer.100251.

[18] M. G. M. Zanjani, H. K. Karegar, H. A. Niaki, and M. G. M. Zanjani, "High Impedance Fault Detection of Distribution Network by Phasor Measurement Units," *Smart Grid and Renewable Energy*, vol. 4, pp. 297–305, Jun. 2013, https://doi.org/10.4236/sgre.2013.43036.

[19] S. Lavanya, S. Prabakaran, and N. A. Kumar, "Literature Review: High Impedance Fault in Power System and Detection Techniques," *Mathematical Statistician and Engineering Applications*, vol. 71, no. 3, pp. 944–958, Jun. 2022.

[20] K. Sekar, K. Kanagarathinam, S. Subramanian, E. Venugopal, and C. Udayakumar, "An Improved Power Quality Disturbance Detection Using Deep Learning Approach," *Mathematical Problems in Engineering*, vol. 2022, 2022, Art. no. 7020979.

[21] S. Lavanya, S. Prabakaran, and N. A. Kumar, "Analysis of High Impedance Fault using Discrete Wavelet Transform Technique," *International Journal of Engineering Trends and Technology*, vol. 70, no. 8, pp. 238–246, 2022, https://doi.org/10.14445/22315381/IJETT-V70I8P225.

[22] A. E. Emanuel, D. Cyganski, J. A. Orr, S. Shiller, and E. M. Gulachenski, "High impedance fault arcing on sandy soil in 15 kV distribution feeders: contributions to the evaluation of the low frequency spectrum," *IEEE Transactions on Power Delivery*, vol. 5, no. 2, pp. 676–686, Apr. 1990, https://doi.org/10.1109/61.53070.

[23] S. Andrews Zachariah, B. Satish Shenoy, J. Jayan, and K. D. Pai, "Experimental investigation on dynamic and static transverse behaviour of thin woven Carbon/Aramid hybrid laminates," *Journal of King Saud University - Engineering Sciences*, vol. 34, no. 4, pp. 273–281, May 2022, https://doi.org/10.1016/j.jksues.2020.09.015.

[24] A. Tariq, K. L. Khatri, M. I. U. Haque, M. A. Raza, S. Ahmed, and M. Muzammil, "Investigation of the Effects of Distributed Generation on Protection Coordination in a Power System," *Engineering, Technology & Applied Science Research*, vol. 11, no. 5, pp. 7628–7634, Oct. 2021, https://doi.org/10.48084/etasr.4338.

[25] N. Narasimhulu, D. V. Ashok Kumar, and M. Vijaya Kumar, "Detection and Classification of High Impedance Fault in Power Distribution System using Hybrid Technique," *Journal of Circuits, Systems and Computers*, vol. 29, no. 8, Jun. 2020, Art. no. 2050118, https://doi.org/10.1142/S0218126620501182.

[26] A. Mahari and H. Seyedi, "High impedance fault protection in transmission lines using a WPT-based algorithm," *International Journal of Electrical Power & Energy Systems*, vol. 67, pp. 537–545, May 2015, https://doi.org/10.1016/j.ijepes.2014.12.022.

[27] C. J. Lee, J. B. Park, J. R. Shin, and Z. M. Radojevie, "A new two-terminal numerical algorithm for fault location, distance protection, and arcing fault recognition," *IEEE Transactions on Power Systems*, vol. 21, no. 3, pp. 1460–1462, Dec. 2006, https://doi.org/10.1109/TPWRS.2006.876646.

[28] R. Eslami, S. H. H. Sadeghi, and H. A. Abyaneh, "A Probabilistic Approach for the Evaluation of Fault Detection Schemes in Microgrids," *Engineering, Technology & Applied Science Research*, vol. 7, no. 5, pp. 1967–1973, Oct. 2017, https://doi.org/10.48084/etasr.1472.

[29] D. khalil Ibrahim, E. S. T. Eldin, E. M. Aboul-Zahab, and S. M. Saleh, "Real time evaluation of DWT-based high impedance fault detection in EHV transmission," *Electric Power Systems Research*, vol. 80, no. 8, pp. 907–914, Aug. 2010, https://doi.org/10.1016/j.epsr.2009.12.019.